Electrophysiology of Flounder Intestinal Mucosa

I. Conductance Properties of the Cellular and Paracellular Pathways

DAN R. HALM, EDWARD J. KRASNY, JR., and RAYMOND A. FRIZZELL

From the Department of Physiology and Biophysics, University of Alabama at Birmingham, Birmingham, Alabama 35294; and Mount Desert Island Biological Laboratory, Salsbury Cove, Maine 04672

ABSTRACT   We evaluated the conductances for ion flow across the cellular and paracellular pathways of flounder intestine using microelectrode techniques and ion-replacement studies. Apical membrane conductance properties are dominated by the presence of Ba-sensitive K channels. An elevated mucosal solution K concentration, $[K]_m$, depolarized the apical membrane potential (ψ_a) and, at $[K]_m < 40$ mM, the K dependence of ψ_a was abolished by 1–2 mM mucosal Ba. The basolateral membrane displayed Cl conductance behavior, as evidenced by depolarization of the basolateral membrane potential (ψ_b) with reduced serosal Cl concentrations, $[Cl]_s$. ψ_b was unaffected by changes in $[K]_s$ or $[Na]_s$. From the effect of mucosal Ba on transepithelial K selectivity, we estimated that paracellular conductance (G_p) normally accounts for 96% of transepithelial conductance (G_t). The high G_p attenuates the contribution of the cellular pathway to ψ_t while permitting the apical K and basolateral Cl conductances to influence the electrical potential differences across both membranes. Thus, ψ_a and ψ_b (~60 mV, inside negative) lie between the equilibrium potentials for K (76 mV) and Cl (40 mV), thereby establishing driving forces for K secretion across the apical membrane and Cl absorption across the basolateral membrane. Equivalent circuit analysis suggests that apical conductance ($G_a \cong 5$ mS/cm^2) is sufficient to account for the observed rate of K secretion, but that basolateral conductance ($G_b \cong 1.5$ mS/cm^2) would account for only 50% of net Cl absorption. This, together with our failure to detect a basolateral K conductance, suggests that Cl absorption across this barrier involves KCl co-transport.

INTRODUCTION

The intestines of marine teleosts absorb NaCl and water so that ingested seawater can replace osmotic water losses to the environment (20). Excess NaCl absorbed

across the gastrointestinal tract is then excreted, primarily across the gills, which results in net hydration of the extracellular space. Salt absorption across flounder intestine was studied by Field et al. (9), who found evidence of coupling between the absorptive fluxes of Na and Cl, which is consistent with neutral, transcellular NaCl co-transport. They presented a model in which a lumen-positive transepithelial potential difference (ψ_t) of 2–5 mV arises, during absorption, as a diffusion potential across Na-selective tight junctions because of lateral intercellular space NaCl accumulation. Similarly, the threefold excess of Cl over Na absorption observed under short-circuit conditions was ascribed to recycling of absorbed Na to the lumen, across the cation-selective junctions.

Subsequent work has confirmed the junctional cation selectivity required by this model (21). However, studies of unidirectional ion influxes from the mucosal solution into the epithelium are not consistent with 1:1 NaCl entry across the apical membrane (24, 25). Ion-replacement studies reveal coupling between the influxes of Na, Cl, and K, and the kinetics of Rb uptake (a K substitute) as a function of mucosal solution ion concentrations suggest a stoichiometry of 1Na:1K:2Cl. Much of the excess of net Cl over Na transport observed under short-circuit conditions can be attributed to an entry mechanism with this stoichiometry. However, since apical Na/K/Cl co-transport is also electrically neutral, the ionic basis of the lumen-positive ψ_t and net positive current flow from serosa to mucosa during short-circuiting remains undefined.

This report summarizes the electrical properties of the apical and basolateral membranes of flounder intestinal cells. Conventional microelectrodes were used to measure the cellular electrical potential profile during changes in the ionic composition of the bathing solutions. Our findings indicate that the serially arranged conductances of the apical and basolateral membranes are major determinants of the lumen-positive ψ_t, so that paracellular pathways need not account entirely for the transepithelial electrical properties of this tissue.

LIST OF SYMBOLS

I_{sc}	short-circuit current
ψ_t, ψ_a, ψ_b	electrical potential difference across the epithelium, apical membrane, and basolateral membrane, respectively; ψ_a and ψ_b are expressed with reference to the adjacent external media (the mucosal and serosal solutions, respectively) and ψ_t is referenced to the mucosal solution (i.e., $\psi_t = \psi_a - \psi_b$)
R_t, R_a, R_b, R_p	electrical resistance of the epithelium, apical membrane, basolateral membrane, and paracellular pathway, respectively
G_t, G_a, G_b, G_p	electrical conductance $(1/R)$ of the epithelium, apical membrane, basolateral membrane, and paracellular pathway, respectively; a superscript is used to identify a partial ionic conductance
f_a^R, f_b^R	fractional apical $[R_a/(R_a + R_b)]$ or basolateral $[R_b/(R_a + R_b)]$ membrane resistance; f_a^R is obtained as $\Delta\psi_a/\Delta\psi_t$ in response to a transepithelial constant current pulse; $f_b^R = (1 - f_a^R)$
E_a, E_b, E_p	electromotive force (emf) across the apical membrane, basolateral membrane, and paracellular pathway, respectively

METHODS

Tissue and Solutions

Intestinal tissue was obtained from winter flounder, *Pseudopleuronectes americanus*, 200–600 g, caught in nets off Mount Desert Island, ME. The fish were kept in tanks of running seawater at 15°C for at least 3 d before use to allow uniform emptying of the intestinal lumen. The small intestinal mucosa was stripped of underlying smooth muscle and mounted horizontally between two halves of a Plexiglas chamber with an aperture of 0.13 cm^2; the serosal surface was supported by nylon mesh. Ringer's solutions saturated with room air continuously flowed past both surfaces of the tissue (single pass), driven by gravity feed from reservoirs maintained at 15°C.

The composition of the standard (control) Ringer's solution was (mM): 165 Na, 170 Cl, 5 K, 2 (HPO_4-H_2PO_4), 1.1 Mg, 1.2 Ca, 5 EPPS (N-[2-hydroxyethyl]-piperazine-N'-3-propane sulfonic acid), and 5 glucose (serosal) or 5 mannitol (mucosal solution). The pH was adjusted to 8.0 with NaOH and the solutions were gassed with room air.[1] For ion-substitution experiments, Na replaced K, gluconate replaced Cl, and N-methyl-D-glucamine (NMG) replaced Na.

Intracellular Recording

Conventional microelectrodes were used to determine the electrical potential of the cell interior with reference to the mucosal solution, ψ_a. They were fabricated using a micropipette puller (PN-3, Narishige, Tokyo, Japan), filled with 0.5 M KCl and connected, via an Ag-AgCl junction, to an electrometer (F23-B, W-P Instruments, Inc., New Haven, CT). Their tip resistances, measured in 0.5 M KCl, ranged from 20 to 50 MΩ; the tapered shank was 5–8 mm in length. The tip diameter was 0.2–0.3 μm, as judged by scanning electron microscopy (performed by Dr. D. R. DiBona).

Single-barreled, Cl-selective microelectrodes were fabricated and calibrated as described previously (7). Sequential or simultaneous conventional and Cl-selective electrode recordings were obtained in the steady states before and after changing experimental conditions. Simultaneous recordings were made using an electrometer (FD-223, W-P Instruments, Inc.) with electrodes spaced within 1 mm of each other to take advantage of the minimal variation observed when repetitive ψ_a values were obtained in this manner (reference 5; see below).

The transepithelial electrical potential difference (ψ_t) was measured with calomel electrodes placed in the exit ports of the chamber perfusion lines. On command of a voltage clamp, bipolar square-wave pulses of direct current (0.5–1 s duration) were passed across the tissue from Ag-AgCl electrodes implanted in each half-chamber. This permitted measurement of the transepithelial (R_t) and fractional (f_a^R, f_b^R) resistances. Values were corrected for I-R drops in the adjacent external media.

Our criteria for a successful impalement were (6): (*a*) an abrupt negative deflection of the potential sensed by the microelectrode tip that reached a plateau value, (*b*) maintenance of the plateau value with no more than 2 mV variation for at least 30 s, and (*c*) a return to the original baseline when the tip was retracted or spontaneously dislodged, which indicated no change in tip potential.

[1] Previous studies were carried out using HCO_3-containing Ringer's at pH 8.0 when gassed with 1% CO_2 (9, 10). However, normal rates of NaCl absorption are observed in nominally HCO_3- and CO_2-free media if the external pH is maintained at 8.0 (34).

An Equivalent Electrical Circuit Model

Expressions for the electrical potential differences across each resistive barrier of the equivalent electrical circuit illustrated in Fig. 1 can be derived from analysis of the voltage divider relations (32), and yield:

$$\psi_t = -[(R_a + R_b)/\Sigma R]E_p - (R_p/\Sigma R)(E_a - E_b); \tag{1}$$

$$\psi_a = -[(R_b + R_p)/\Sigma R]E_a - (R_a/\Sigma R)(E_b + E_p); \tag{2}$$

and

$$\psi_b = -[(R_a + R_p)/\Sigma R]E_b - (R_b/\Sigma R)(E_a - E_p), \tag{3}$$

where $\Sigma R = R_a + R_b + R_p$. The sign conventions applied to the electromotive forces are as shown in Fig. 1.
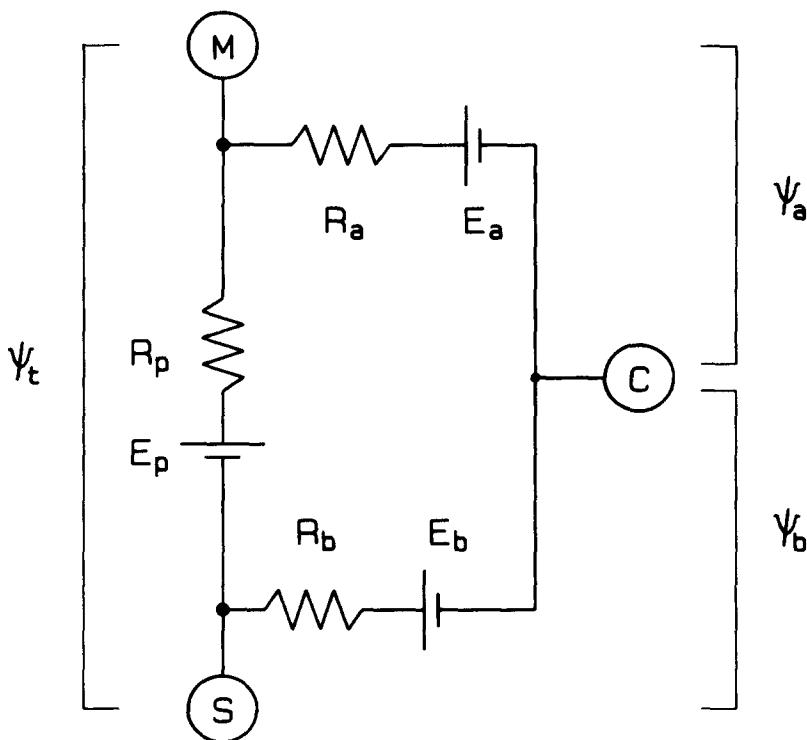

FIGURE 1. An equivalent electrical circuit model for flounder intestinal epithelium. See the List of Symbols for definition of terms.

It is sometimes useful to express ψ_t in terms of the cellular (G_c) and paracellular (G_p) conductances for ion flow:

$$\psi_t = -(G_p/G_t)E_p - (G_c/G_t)(E_a - E_b), \tag{4}$$

where $G_t = (G_c + G_p)$ is the instantaneous electrical conductance of the tissue $(1/R_t)$. It is also convenient to express ψ_a and ψ_b in terms of the measured ψ_t and fractional apical and basolateral membrane resistances:

$$\psi_a = -f_b^R E_a - f_a^R (E_b - \psi_t); \tag{5}$$

$$\psi_b = -f_a^R E_b - f_b^R (E_a + \psi_t). \tag{6}$$

These expressions form the basis for estimating the relative contributions of cellular and paracellular conductances to the transepithelial electrical properties (see below) and facilitate discussion of the ionic basis of the cellular electrical potential profile.

RESULTS

In this section, we analyze the conductance properties of the limiting membranes and paracellular pathway using ion-replacement studies. The behavior of the cellular electrical potential profile with ion replacement is most readily understood by first considering the contribution of paracellular conductance (G_p) to the total tissue conductance (G_t). The relative electrical leakiness of the paracellular pathway determines the extent to which the apical and basolateral membrane potentials interact electrically during changes in a single transmembrane ion gradient or emf (31, 32).

Analysis of the Equivalent Circuit: Paracellular Conductance

The ratio of paracellular to total tissue conductance (G_p/G_t) was evaluated using diffusion potentials generated by transepithelial (Na:K) gradients in the presence and absence of mucosal Ba. Since the only detectable apical membrane conductance is that to K (see below), a blocker of apical K conductance effectively eliminates the contribution of cellular pathways to G_t, permitting estimation of G_p/G_t from Eq. 4.

Under normal conditions, bi-ionic potentials resulting from gradients of Na and K across the epithelium reflect emf's established across both the cellular and paracellular pathways. Accordingly, short-term replacement of mucosal solution Na by K alters ψ_t by changing E_a and E_p but not E_b. If the conductances are voltage- and concentration-independent for small perturbations, the change in ψ_t that accompanies mucosal Na by K replacement is given by:

$$\Delta\psi_t = -(G_p/G_t)\Delta E_p - (G_c/G_t)\Delta E_a^K, \tag{7}$$

where E_a in Eq. 4 has been approximated by E_a^K. Since tissue conductance is high (~ 25 mS/cm^2), relative changes in G_p and G_c accompanying ion replacement are assumed to be negligible.

As implied above, inhibition of apical membrane K conductance by mucosal Ba removes the contribution of E_a^K to ψ_t by effectively eliminating G_c/G_t, so that Eq. 7 reduces to:

$$\Delta\psi_t^{Ba} = -\Delta E_p. \tag{8}$$

Substituting $G_c/G_t = (1 - G_p/G_t)$ and Eq. 8 into Eq. 7 provides an estimate of the contribution of G_p to G_t:

$$G_p/G_t = (\Delta E_a^K + \Delta\psi_t)/(\Delta E_a^K + \Delta\psi_t^{Ba}). \tag{9}$$

Values of ψ_t were recorded during substitution of K for Na in the presence and absence of mucosal Ba. Estimates of the lumped epithelial permeability ratio (P_K/P_{Na}) were calculated using the Goldman-Hodgkin-Katz equation and the

ratio P_{Cl}/P_{Na}, determined from diffusion potential measurements in another study (21).[2] The results are presented in Table I.

The adequacy of this approach depends on a near-complete block of apical K conductance by mucosal Ba. This is revealed most directly by its effect on ψ_a and f_a^R (shown below), but it also is evident from the effect of Ba on transepithelial K selectivity (Table I). The observed decrease in P_K/P_{Na} is consistent with Ba blockade of the K-selective cellular conductance. The P_K/P_{Na} ratio in the presence of Ba is equal to the ratio of the aqueous diffusion coefficients of these ions ($\lambda_K/\lambda_{Na} = 1.5$), and suggests that the paracellular route provides a nonrestrictive, watery pathway for cation diffusion between cells.

The results of this analysis provide an estimate of 0.96 for G_p/G_t (range 0.85–0.99). This is similar to the value obtained for *Necturus* gallbladder by Suzuki et al. (36). The relative conductance of the paracellular pathway is high, which confirms impressions gained from the low values of ψ_t and R_t that characterize this epithelium as "electrically leaky."

TABLE I

Na:K Diffusion Potentials: an Estimate of G_p/G_t

	$\Delta\psi_t$		P_K/P_{Na}			
$\Delta[K]_m$	Control	Mucosal barium	Control	Mucosal barium	G_p/G_t	n
mM	*mV*	*mV*				
5 → 15	0.9±0.4	0.3±0.1	1.8±0.4	1.3±0.1	0.98±0.01	4
5 → 40	3.7±0.6	1.7±0.2	2.0±0.2	1.4±0.1	0.96±0.01	14
5 → 100	8.2±2.0	4.9±0.7	1.9±0.3	1.5±0.1	0.95±0.03	5

Means ± SEM for n tissues. P_K/P_{Na} represents the transepithelial permeability ratio, derived as described in the text. $[Na]_m + [K]_m = 170$ mM; $[Ba]_m = 2$ mM.

Table II provides estimates of the conductances of the limiting membranes and paracellular pathway. Knowledge of G_p/G_t permits calculation of G_c and, from the measured f_a^R, of G_a and G_b. The values obtained for the group of 14 tissues exposed to 40 mM K (Table I) were used in the calculations because the sample size was large, and G_p/G_t was representative of the other two groups. Comments on the G_a and G_b values appear in the Discussion.

Another Attempt to Estimate Paracellular Conductance

One approach to the determination of the equivalent resistances of the apical and basolateral membranes involves the measurement of changes in G_t and f_a^R induced by an agent that specifically alters only one of the resistive barriers. The time courses of changes in G_t and f_a^R induced by mucosal Ba are shown in Fig. 2A. A specific block of G_a^K would permit estimation of paracellular conductance from the intercept of a plot relating G_t to f_b^R (22) during the action of mucosal Ba:

[2] Diffusion potentials arising from isosmotic replacement of mucosal solution NaCl by mannitol provided an average P_{Na}/P_{Cl} value of 5.0 ± 0.2 ($n = 13$).

$$G_t = G_p + G_b f_b^R. \tag{10}$$

However, as shown in Fig. 2B, the observed relation between G_t and f_b^R is nonlinear. The dashed line is that expected for a paracellular conductance that contributes 96% of the total G_t (as suggested by the diffusion potential analysis discussed above). Since the G_p estimated as 0.96 G_t (intercept of the dashed line) is larger than G_t after addition of Ba, Ba must have decreased G_p. In 12 experiments similar to that illustrated in Fig. 2, this decrease in G_p was 3 ± 1% (which corresponds to an increase in resistance of only 1.4 ± 0.3 $\Omega \cdot cm^2$).[3] This small effect of Ba on G_p obscures the determination of G_c using this approach, but probably does not alter the relative paracellular cation selectivities (P_K/P_{Na}) that contribute to the analysis of G_p/G_t from transepithelial diffusion potentials. However, the results of Fig. 2B indicate that attempts (17) to define cellular conductances from the difference in G_t before and after addition of Ba can yield misleading results.

TABLE II
Estimation of Conductances

Measured values	G_t	f_a^R	I_{sc}	ψ_a	
	mS/cm^2		$\mu A/cm^2$	mV	
	28.0±1.6	0.24±0.04	66±8	−59±2	
Calculated values	G_p/G_t	G_c	G_a	G_b	G_p
		mS/cm^2	mS/cm^2	mS/cm^2	mS/cm^2
	0.96±0.01	1.1±0.3	5.2±1.2	1.5±0.4	26.8±1.6

Means ± SEM for the 14 tissues that make up the center row of data in Table I.

Influence of G_p/G_t on the Determination of Cellular Conductance Properties

The electrical consequence of the low-resistance paracellular (shunt) pathway is that the apical and basolateral membrane emf's (E_a and E_b, Fig. 1) are connected to the intracellular point of measurement virtually in parallel, so that the emf's of both membranes influence ψ_a and ψ_b. The actual ψ_a and ψ_b values are determined primarily by the emf of the more conductive membrane, as Eqs. 5 and 6 indicate. The tendency for the emf's of both membranes (depending on their relative conductances) to influence ψ_a and ψ_b is a direct consequence of current flow through the paracellular pathway, caused by the high G_p/G_t, and is common to leaky epithelia (32).

Fig. 3 provides a histogram of ψ_a values obtained under control conditions (closed circles). These values are distributed around a mean of −60 ± 8 mV

[3] A curvature in the relation of G_t to f_b^R could result from impalement damage, since f_b^R would approach a limiting value less than unity (f_b^R greater than zero) if a significant nonselective apical conductance is introduced with impalement. However, a similar curvature in the relation of G_t to f_a^R was noted in tissues where the final f_a^R induced by mucosal Ba was in excess of 0.9. The data of Fig. 2 are more representative of all tissues studied.

(SD). The variance is primarily between tissues since impalements from single tissues had an average standard deviation of only 3 mV (see also reference 5). A group of lower ψ_a values (filled triangles, Fig. 3) were recorded from three tissues. Their significance will be discussed below.
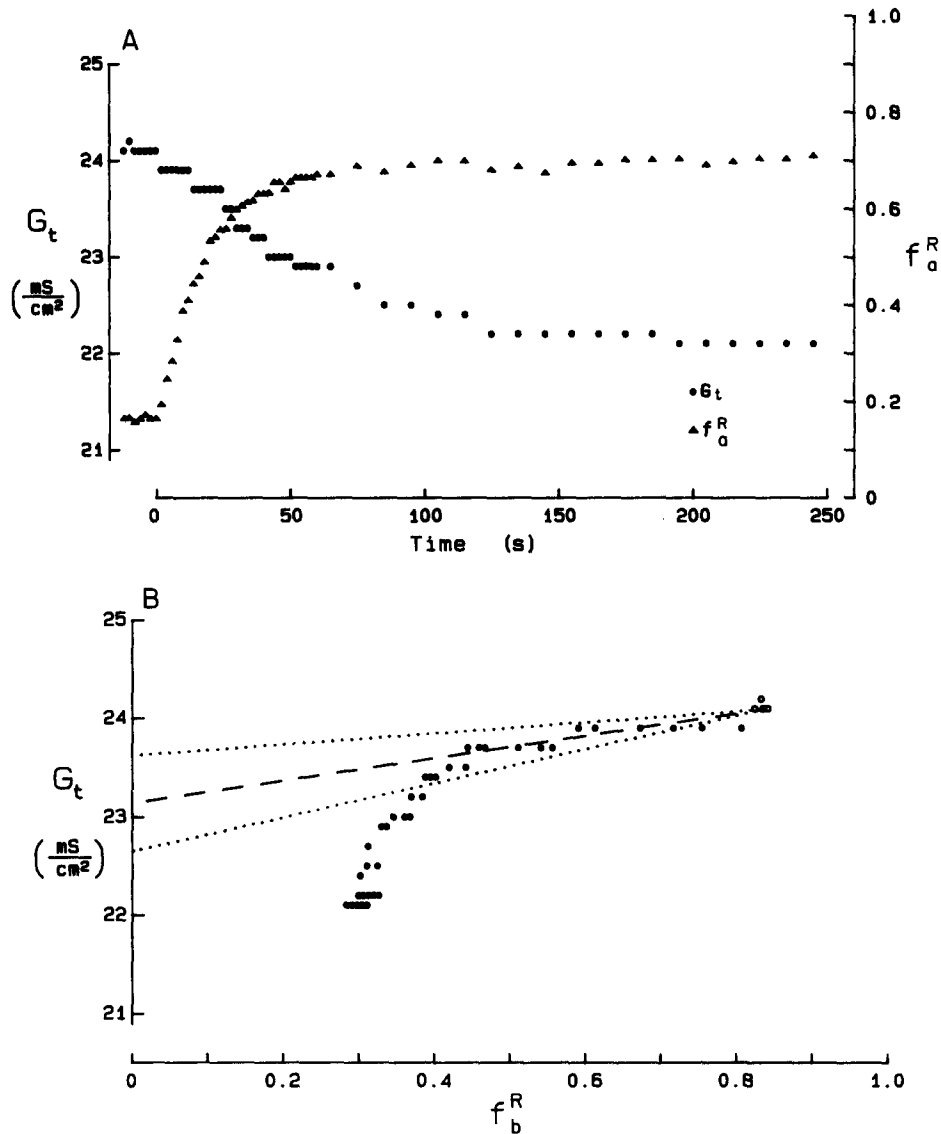

FIGURE 2. Effects of 2 mM mucosal Ba on G_t and fractional membrane resistances. (A) Time course of G_t (●) and f_a^R (▲); Ba was added to the mucosal solution at zero time. (B) Relation of G_t to f_b^R during the action of mucosal Ba. Open circles (upper right) represent control values. The dashed and dotted lines define the relation and confidence interval expected from the data of Table I (see text for further discussion).

The frequency of occurrence for the fractional apical membrane resistance is shown in Fig. 4. The mean value of f_a^R was 0.2 ± 0.1 (SD) in control tissues, so that the apical membrane is normally about four times more conductive than the basolateral membrane. Since low f_a^R values (average 0.2) were associated with high ψ_a values (average −60 mV), impalement damage is not responsible for the low relative apical membrane resistances obtained in these studies.

The low f_a^R values obtained under control conditions indicate that E_a is the primary determinant of ψ_a and ψ_b (Eqs. 5 and 6). Moreover, the conductance properties of the apical membrane are readily detected during replacement of conductive bathing ions, whereas those of the basolateral membrane tend to be
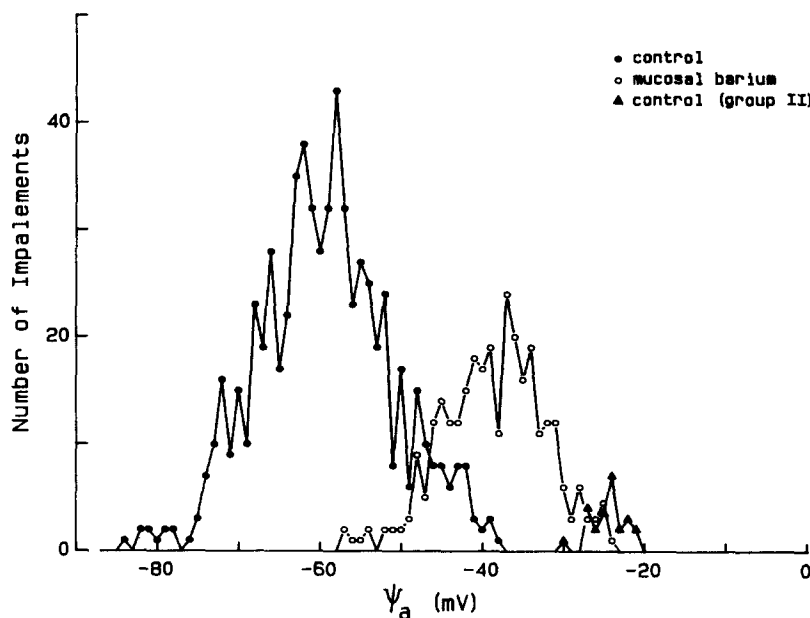

FIGURE 3. Histogram of ψ_a values recorded under control conditions (●, ▲) and in the presence of 1–2 mM mucosal Ba (○). The control values designated by the filled triangles (group II) represent 3% of the population; their significance is discussed in the text. The numbers of tissues and impalements, respectively, were 76 and 668 and 3 and 25 for the large and small control populations, and 47 and 299 for the Ba-treated tissues.

obscured by the low f_a^R. A more reliable indication of basolateral conductance properties can be achieved after experimental adjustment of f_a^R using a blocker of apical conductance pathways (see below).

Apical Membrane Conductance Properties

Fig. 5A shows the response of ψ_a and ψ_t to a change in $[K]_m$ from 5 to 40 mM (K replaced Na). Depolarization of ψ_a is consistent with the presence of apical membrane K conductance pathways, as implied by the preliminary findings of Helman and Beyenbach (18). The concomitant change in ψ_t with elevated $[K]_m$ reflects the overall K selectivity of the epithelium, as discussed earlier.
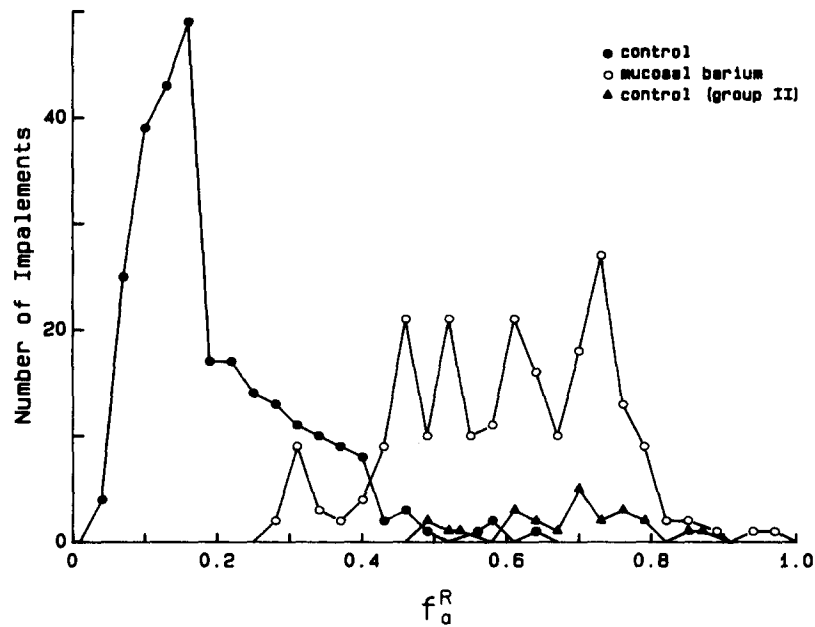
FIGURE 4. Histogram of f_a^R values recorded under control conditions (●, ▲) and in the presence of 2 mM mucosal Ba (○). The number of tissues and impalements, respectively, were 38 and 285 and 2 and 16 for the large and small control populations, and 30 and 225 for the Ba-treated tissues.
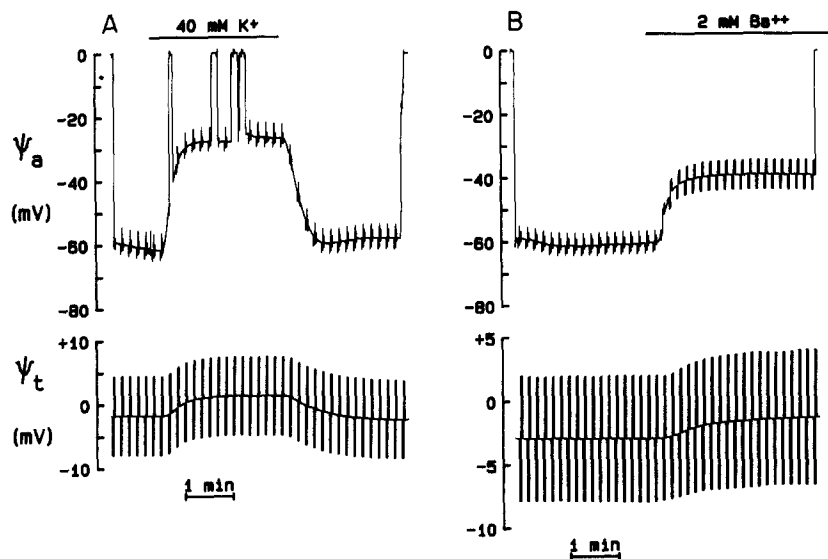

FIGURE 5. Representative recordings of the electrical response to (A) elevation of $[K]_m$ from 5 to 40 mM and return, and (B) addition of 2 mM Ba to the mucosal solution. Several impalements are illustrated in record A, one in record B. Deflections in ψ_a and ψ_t result from the passage of bipolar constant-current pulses across the epithelium to obtain f_a^R; see text.

The addition of Ba to the mucosal solution also depolarized ψ_a and reduced ψ_t by ~50% (Fig. 5 B). The effect of mucosal Ba on the distribution of ψ_a and f_a^R values is illustrated in Figs. 3 and 4 (open circles). The results were obtained using either 1 or 2 mM Ba, which is a maximally effective concentration when the bathing media contain 5 mM K (i.e., the addition of 1, 2, or 5 mM Ba to the mucosal solution produced equal depolarizations of ψ_a). The average decrease in ψ_a in 36 paired studies was 21 ± 1 mV (SEM).

The K conductance properties of the apical membrane are illustrated by the dependence of ψ_a on $[K]_m$. Fig. 6 shows that logarithmic increases in $[K]_m$ from the normal value of 5 mM depolarize ψ_a in a linear manner, which is consistent with simple K electrode behavior of the apical membrane potential. The slope
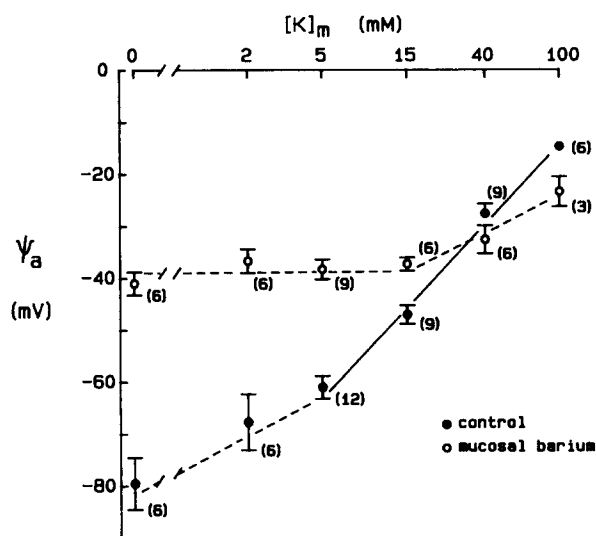

FIGURE 6. Relation of ψ_a to $[K]_m$ in the presence (O) and absence (●) of 2 mM mucosal Ba. Values were obtained from records like that of Fig. 5A. Each mean ± SEM was obtained from the number of tissues given in parentheses. See text for further details.

of this relation is 37 ± 2 mV/decade $[K]_m$, which is less than the ideal value of 57 mV/decade at 15°C. This is expected in a leaky epithelium, where ψ_a is influenced by both E_a and E_b (Eq. 5).

Under control conditions, the relation between ψ_a and $[K]_m$ deviates from linearity below 5 mM K (Fig. 6). Similar results have been obtained for *Necturus* gallbladder (31). The curvature at low $[K]_m$ could reflect our inability to lower [K] in the apical unstirred layer below a minimal level. Extrapolation of the solid line in Fig. 6 to the ψ_a value observed in nominally K-free media (−80 mV) suggests that 1–2 mM K is present near the apical membrane under these conditions, which could result from K secretion across apical K conductance pathways (10). In addition, f_a^R increases when $[K]_m$ is reduced below 5 mM (not shown), so that the influence of E_a^K on ψ_a is also attenuated (conversely, the

influence of E_b on ψ_a is enhanced; Eq. 5). Thus, the curvature at low $[K]_m$ probably reflects both decreased apical conductance (caused by depletion of the permeant ion) and a limiting K concentration in the apical unstirred layer.

Fig. 6 also shows that addition of 2 mM Ba to the mucosal solution eliminates the K dependence of ψ_a at values of $[K]_m$ below 40 mM. The data reported in the companion paper (16) indicate that the influence of $[K]_m$ on f_a^R is also abolished over this range of concentrations. These findings are consistent with the ability of Ba to interfere with both epithelial (10, 12, 13, 19, 26, 30) and neuronal (1, 8) K channels and suggest that when $[K]_m$ is in the physiological range of concentrations, the blockade of G_a^K by mucosal Ba is nearly complete. Ba also increases f_a^R to 0.6 ± 0.1 (SD) (Fig. 4) and thereby decreases the influence of E_a on ψ_a (Eq. 5).[4] With a constant mucosal Ba concentration and $[K]_m$ in excess of 40 mM, ψ_a again displays K dependence, and f_a^R decreases as $[K]_m$ is raised. Thus, the blockade of G_a^K by mucosal Ba is reduced at sufficiently elevated $[K]_m$, which probably results from competition between K and Ba for channel occupancy, as observed by Armstrong et al. (1) in squid giant axon.

Additional support for K selectivity of the apical membrane conductance is twofold. First, the relation between ψ_a and $[K]_m$ can be corrected for the effects of electrical shunting via the paracellular pathway using measured values of f_a^R, ψ_a, and ψ_t, together with Eq. 5, to obtain E_a values at various $[K]_m$. The resulting relation between E_a and $[K]_m$ displays a slope of 51 ± 2 mV/decade, which reflects near-ideal K electrode behavior. Second, the addition of 0.5 mM Ba to the mucosal solution only partially reduced G_a^K, so that the influence of other possible apical membrane conductances on ψ_a should be accentuated. Nevertheless, the relation of ψ_a to $[K]_m$, which displays a slope of 20 ± 1 mV/decade in the presence of 0.5 mM Ba, yielded a value of 47 ± 2 mV/decade when the

[4] One finding that is difficult to reconcile with this conclusion is the f_a^R observed in the presence of mucosal Ba. Although Ba eliminates the K dependence of ψ_a at physiological $[K]_m$ (Fig. 6), the average f_a^R was 0.6 ± 0.1, not unity (Fig. 4). Our findings suggest that this is not because of the presence of other apical conductances (see discussion to follow), but may be attributed to the effects of a distributed resistance along the lateral intercellular space (2). The equivalent circuit of Fig. 1 assumes that the series resistance of the bathing solutions can be compensated using the external correction circuit of the voltage clamp. However, a long, narrow lateral space imposes a distributed resistance in series with the equivalent resistance of the lateral cell membrane. This can result in an underestimate of f_a^R, since current that flows across the basolateral membrane must also flow across this series resistance. The geometry of flounder intestinal cells ($\sim$50 μm long $\times$ 3 μm wide) suggests that a distributed paracellular resistance could affect the measured f_a^R.

The analysis of Boulpaep and Sackin (2) provides an empirical description of distributed resistance, which permits estimation of the true f_a^R from the measured f_a^R. The resistance of the lateral intercellular space, R_{LIS}, can be approximated from tissue geometry. In flounder intestine, this space is $\sim$50 μm long and 0.01–1.0 μm wide (depending on transport conditions) and, assuming a square array of cells, the linear extent of junctions is $\sim$10^4 cm/cm^2. Taking the solution resistivity as 100 $\Omega \cdot$cm^2, R_{LIS} ranges from 0.7 (spaces distended) to 50 $\Omega \cdot$cm^2 (spaces collapsed). During transport, the spaces are open (9), which suggests that the contribution of R_{LIS} to R_p is <5%. Since the resistance of the tight junctions is considerably lower than that of the apical membrane, the f_a^R measured under control conditions probably underestimates the actual value by $\sim$10% (2). This error becomes more pronounced as f_a^R increases, as with mucosal Ba, but it is difficult to estimate precisely.

attenuation by paracellular shunting was corrected. This suggests that apical conductance to ions other than K is normally negligible.

Our attempts to evaluate apical Na and Cl conductance properties yielded results whose interpretation was not straightforward. Briefly, complete replacement of Na by NMG or Cl by gluconate elicited a relatively slow (3–5 min) hyperpolarization of ψ_a that averaged ~15 mV. While the effect of Na replacement on ψ_a is suggestive of Na conductance behavior, the result obtained with Cl-free mucosal solutions is anomalous. We would expect a depolarization of ψ_a with decreased $[Cl]_m$ if the apical Cl conductance were significant, but hyperpolarization was consistently observed. In addition, the response to decreased $[Na]_m$ was not mimicked by mucosal amiloride (0.01–1 mM), as is normally
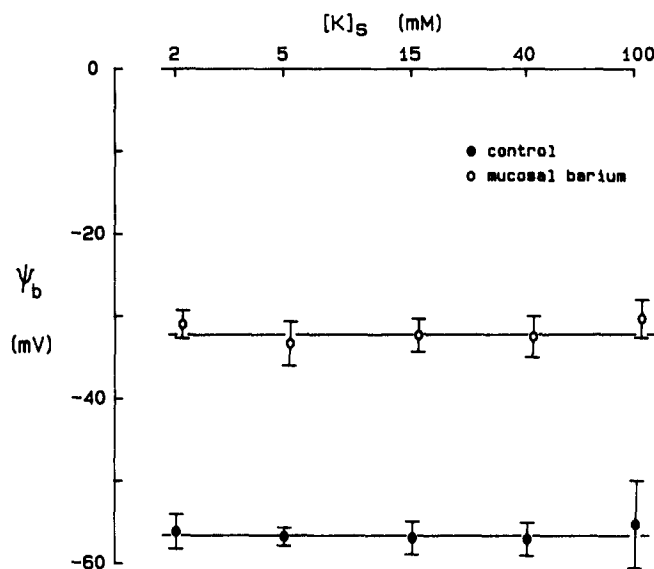

FIGURE 7.   Relation of ψ_b to $[K]_s$ in the presence (O) and absence (●) of 2 mM mucosal Ba. Each value represents the mean ± SEM of records obtained from three tissues.

characteristic of epithelia possessing apical Na conductance (4, 23). The hyperpolarizations elicited by Na- or Cl-free media are mimicked by bumetanide (16, 24) and appear to result from inhibition of coupled NaCl absorption. Our analysis of these findings is the subject of the companion paper (16).

Basolateral Membrane Conductance Properties

The finding that the normally low values of f_a^R could be elevated by mucosal Ba was exploited to enhance the influence of E_b on ψ_b during our attempts to evaluate the conductance properties of the basolateral membrane (see Eq. 6 and the discussion on p. 851). Nevertheless, Fig. 7 shows that ψ_b was not affected by changes in serosal solution K concentration in either the presence or absence of mucosal Ba. In addition, serosal Ba had no effect on the electrical potential

profile (35) or on the rate of active Rb (a K substitute) secretion across flounder intestine under short-circuit conditions (10). These findings indicate that a basolateral membrane K conductance, characteristic of most epithelia, cannot be detected in flounder intestinal cells. Changes in serosal solution Na concentration also had no effect on ψ_b (35).

Evidence of basolateral membrane Cl conductance behavior is illustrated in Fig. 8. Reductions in serosal solution Cl concentration depolarized ψ_b. These studies were also conducted in the presence of 2 mM mucosal Ba to increase f_a^R and enhance the dependence of ψ_b on E_b (Eq. 6). The finding that the slope of the relation between ψ_b and $\log[Cl]_s$ is less than that predicted for absolute Cl selectivity is, again, a reflection of electrical coupling between the limiting membranes since f_a^R was 0.7, not unity, despite the presence of mucosal Ba.
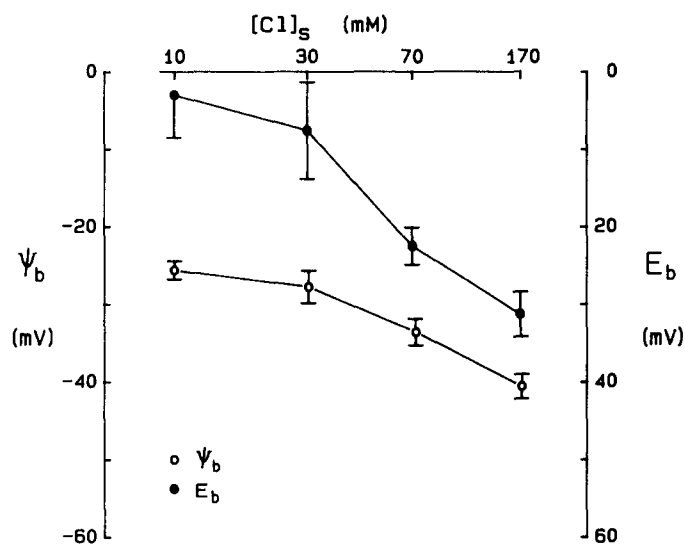

FIGURE 8. Relation of ψ_b (O) and E_b (●) to $[Cl]_s$ in the presence of 2 mM mucosal Ba. E_b values were calculated using the ψ_b data and Eq. 6. Each value is the mean ± SEM of at least three impalements at each $[Cl]_s$ in a representative experiment.

As in the K-replacement studies, the measured values of ψ_b can be corrected for the effects of electrical shunting (Eq. 6). In this manner, the dependence of E_b on $[Cl]_s$ can be examined; it is also shown in Fig. 8. Over the range 30–170 mM $[Cl]_s$, the slope improves to 50 ± 3 mV/decade, which suggests that G_b^{Cl} is the major determinant of basolateral membrane conductance. The tendency of these relations to plateau at low $[Cl]_s$ may reflect the difficulty in lowering the Cl concentration of the unstirred serosal space (particularly the lateral intercellular space) below a minimal level. It can be concluded that G_b^{Cl} had been overlooked previously (35) for two reasons: first, the low fractional resistance of the apical membrane normally attenuates the influence of E_b^{Cl} on ψ_b. Second, difficulties can arise in attempts to demonstrate Cl conductance behavior by complete

replacement with an impermeant anion. This procedure removes the conductive ion, which further increases basolateral membrane resistance, reduces f_a^R, and decreases the influence of E_b^{Cl} on ψ_b (or, conversely, enhances the influence of E_a^K).

The notion that basolateral conductance properties are dominated by G_b^{Cl} is supported by the "limiting" values of ψ_a obtained in the presence of mucosal Ba. As discussed earlier, blockade of the apical K channels permits other cellular conductances to influence ψ_a, as expressed by Eq. 5. Since apical conductance to ions other than K appears to be negligible, ψ_a (and ψ_b) will approach E_b as G_a^K decreases. The chemical potential difference for Cl across the basolateral membrane (E_b^{Cl}) determined by Duffey et al. (6) using Cl-selective microelectrodes was 41 $\pm$ 3 mV. This is in excellent agreement with the value of ψ_a (-39 ± 1 mV) obtained in the presence of mucosal Ba (Figs. 3 and 6).

This conclusion is supported by the data presented in Table III. Intracellular Cl activities (a_c^{Cl}) were determined in the presence and absence of mucosal Ba. Under control conditions, a_c^{Cl} and E_b^{Cl} were in excellent agreement with values obtained previously (6). A 16-mV difference between E_b^{Cl} and ψ_b provides the

TABLE III

*Effects of Mucosal Barium on the Electrical Potential
Profile and Cell Cl Activities in Flounder Intestine*

	ψ_t	ψ_a	f_a^R	a_c^{Cl}	E_b^{Cl}	ψ_b
	mV	mV		mM	mV	mV
Control	-2.5 ± 0.2	-58 ± 1	0.42 ± 0.06	27 ± 3	40 ± 3	-56 ± 2
Barium	$-1.6\pm0.3*$	$-30\pm4*$	$0.81\pm0.05*$	40 ± 6	31 ± 4	$-29\pm4*$

Means $\pm$ SEM of five experiments. Barium (2 mM) was added to the mucosal solution alone. E_b^{Cl} was calculated as $-RT/F \ln(a_c^{Cl}/a_s^{Cl})$ where the Cl activity of the serosal solution (a_s^{Cl}) was 128 mM.
* $P < 0.05$ compared to control value.

driving force for Cl exit across the basolateral membrane in this series of experiments. In the presence of mucosal Ba, ψ_b depolarized (via electrical coupling to ψ_a), so that the difference between E_b^{Cl} and ψ_b was eliminated. The approach of ψ_a and ψ_b toward E_b^{Cl} after apical K channel blockade supports the conclusion that the basolateral membrane is primarily conductive to Cl.

One of the tissues with spontaneously low ψ_a and high f_a^R (Figs. 3 and 4) was exposed to Cl-free serosal solutions (gluconate replacement). The effect on the electrical potential profile and on the fractional resistance of the basolateral membrane (f_b^R) is illustrated in Fig. 9. The cell interior became electrically positive with respect to both the mucosal and serosal solutions during serosal Cl replacement, which is consistent with a pronounced effect of E_b^{Cl} on the electrical potential profile. In addition, f_b^R increased when Cl was replaced by gluconate, as expected for a decrease in permeant ion concentration. The response is especially dramatic because of the spontaneously high values of f_a^R (low f_b^R). This confers, without experimental intervention, the conditions appropriate for detection of basolateral conductance properties.

Without explicit analysis of the individual membrane resistances, we cannot discern whether the low ψ_a and high f_a^R of these tissues arise from decreased G_a^K, increased G_b^{Cl}, or both. They exhibit suppressed ψ_a-$[K]_m$ relations (11 mV/decade $[K]_m$), but this could result from enhanced basolateral Cl conductance as well as reduced G_a^K. More extensive studies are precluded by the frequency with which these tissues are encountered (one in 40). Nevertheless, their ψ_t values averaged -2.9 ± 0.6 mV (within the normal range), which indicates that tissue viability was not compromised. The physiologic factors responsible for their modified conductance properties are unknown.
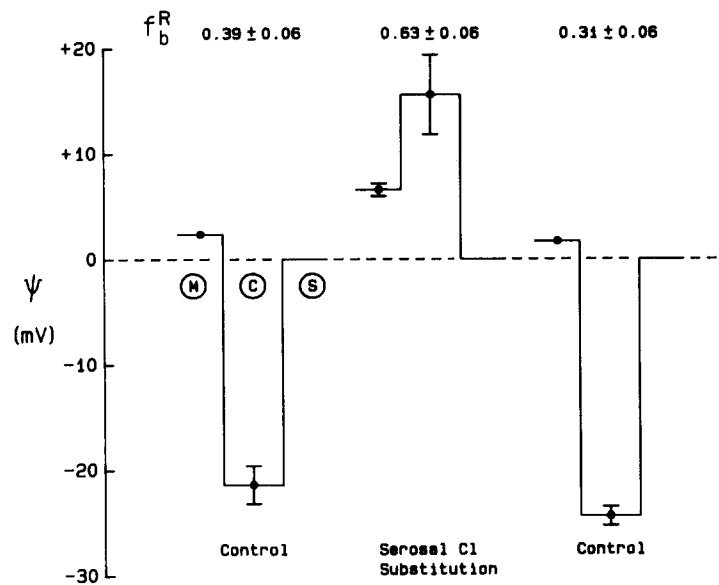

FIGURE 9. Response of the cellular electrical potential profile and f_a^R to a Cl-free serosal solution (gluconate replacement). This tissue displayed spontaneously low ψ_a and high f_a^R values (Figs. 3 and 4, filled triangles) characteristic of low G_a^K or high G_b^{Cl}. Note that in this instance the mucosal solution and cell voltages are referenced to the serosal solution to afford direct comparison of ψ_b values during serosal Cl replacement. At least three impalements were obtained under each condition.

DISCUSSION

In this section, we describe a cellular model for electrolyte transport across flounder intestine that is compatible with our findings. Within the framework of this model, we discuss: (a) the conductance properties of the apical and basolateral membranes, (b) the contribution of cellular and paracellular conductances to the electrical potential profile, (c) the influence of the paracellular pathway on the driving forces for diffusional K and Cl exit across the limiting cell membranes, (d) the adequacy of apical and basolateral membrane conductances in accounting for these movements, and (e) modifications in electrolyte transport induced by altering G_a^K.

Cellular Model for Ion Transport

The model illustrated in Fig. 10 incorporates our current understanding of the conductance properties of the limiting cell membranes. As discussed earlier, the primary mechanism for salt entry across the apical membrane is Na/K/Cl co-transport. Na entering via this process is subsequently extruded across the basolateral membrane by the Na/K pump, leading to K uptake from the serosal solution. Conductance pathways permit net diffusional exit of K and Cl across the apical and basolateral membranes, respectively. A fraction of basolateral Cl exit appears to involve KCl co-transport for reasons that will be discussed in detail below. This model may also portray the salt-absorptive mechanisms of other epithelia: for example, the diluting segment in *Amphiuma* kidney (27) and the thick ascending limb of rabbit nephron (3, 14, 17). The similarities in electrolyte transport across flounder intestine and thick ascending limb have been noted previously (11).
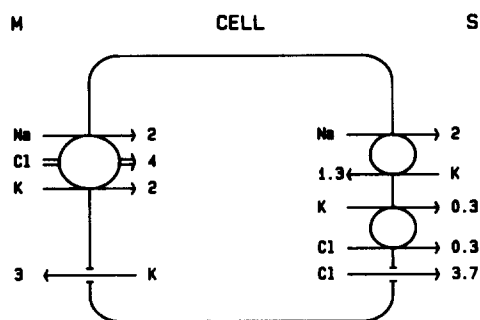
FIGURE 10. Cellular model for electrolyte transport across flounder intestine under control conditions. The values provided for net Na, Cl, and K fluxes (μeq/ cm^2·h) across the apical and basolateral membranes are consistent with prior unidirectional tracer flux determinations (9, 10, 24). The full range of measured K secretion rates (0.5–1.0 μeq/cm^2·h; reference 10) together with mass balance considerations (as in this figure) indicate a net K efflux across the basolateral membrane of 0.3–0.8 μeq/cm^2·h, presumably via KCl co-transport; see Discussion.

Several findings indicate that G_a^K is the only experimentally detectable conductance at the apical membrane. One illustration of this is provided by the dependence of ψ_a (and E_a) on [K]$_m$ and the effects of mucosal Ba on the relation of ψ_a to [K]$_m$ (Fig. 6). The unidirectional K fluxes across flounder intestine, determined under short-circuit conditions, provide evidence of active K secretion (10). Blockade of apical K channels by mucosal Ba reverses the direction of net K transport to absorption. Thus, the direction of net K transport across the apical membrane is determined by the balance between K uptake via Na/K/Cl co-transport and diffusional K exit via apical conductance pathways.

In contrast to its apical counterpart, the basolateral membrane voltage displays no K dependence (Fig. 7). This and other findings suggest that Cl conductance pathways dominate the electrical properties of the basolateral membrane; among

these are the dependence of ψ_b (and E_b) on $[Cl]_s$ (Fig. 8) and the close agreement between E_b^{Cl} and ψ_b after apical K channel blockade (Table III). The role of these conductance pathways in net Cl movement across the basolateral membrane will be discussed below.

The Contribution of Cellular and Paracellular Conductances to Transepithelial Electrical Properties

As discussed in the Introduction, earlier studies attributed the lumen-positive ψ_t across flounder intestine to a NaCl diffusion potential across cation-selective tight junctions (9). However, our findings demonstrate the presence of cellular conductances that permit positive current flow from serosa to mucosa during NaCl absorption (i.e., diffusional exit of K across the apical membrane and of Cl across the basolateral membrane). This permits the emf's operating across the cellular pathway to contribute to the generation of ψ_t, and the extent of their contribution is expressed by Eq. 4. Our estimate of G_c/G_t (0.04 ± 0.01, Table I), together with previously determined values of E_a^K (76 mV) and E_b^{Cl} (41 mV) provide a value of -1.5 ± 0.4 mV for the cellular contribution to ψ_t. This estimate depends strongly on our ability to accurately determine G_c/G_t: a value of 0.08 for G_c/G_t yields a ψ_t of -3 mV, which is in the range of typically recorded ψ_t values (-2 to -5 mV).

Nevertheless, several other findings are consistent with the conclusion that E_a^K and E_b^{Cl} are not the sole determinants of ψ_t. (a) When G_c/G_t approaches zero, as with mucosal Ba, ψ_t should be abolished. However, in the experiments carried out at 5 mM K (see, for example, Fig. 5B), 50% of ψ_t remains after Ba addition. (b) Three tissues displayed spontaneously low ψ_a (Fig. 3) and high f_a^R (Fig. 4) values and depressed relations of ψ_a to $[K]_m$, but their ψ_t values were in the normal range. (c) The model of Field et al. (9) attributes the threefold excess of Cl over Na absorption, observed under short-circuit conditions, to recycling of transported Na to the mucosal solution via the lateral intercellular spaces and tight junctions. Co-transport of Na/K/Cl across the apical membrane (24) is consistent with a transport stoichiometry of 2Cl:1Na, whereas the ratio of net transport rates is routinely 3:1. This difference in Cl and Na transport rates cannot be explained entirely by our current understanding of events in the cellular pathway.

Our estimate of G_p/G_t, together with Eq. 4, indicates that a paracellular emf would contribute to ψ_t with little attenuation by cellular conductances. Recently determined paracellular P_{Na}/P_{Cl} values (21) require that lateral intercellular space [NaCl] exceed its ambient concentration by 6%, or ~10 mM, to produce a diffusion potential of 1 mV, lumen-positive. Whether the relatively long and narrow lateral intracellular spaces found in this tissue can sustain a NaCl concentration difference of this magnitude across its apical tight junction boundary will be difficult to resolve.

Effect of the High G_p on Cellular Transport Processes

One consequence of the highly conductive paracellular pathway is its influence on the driving forces for K and Cl transport across the limiting cell membranes.

As stated earlier, electrical shunting of the emf's at each membrane, via current flow through the paracellular pathway, causes ψ_a and ψ_b to be influenced by both E_a and E_b (see Eqs. 5 and 6). The high selectivity of the apical membrane for K, and of the basolateral membrane for Cl, requires this "cross-talk" for generation of the driving forces for net K and Cl diffusion across the opposing cell membranes. That is, if E_a^K were the sole determinant of ψ_a, K would be distributed at equilibrium across the apical membrane and net secretion via apical K channels would be precluded. A similar conclusion would apply to diffusional Cl exit across the basolateral membranes if ψ_b were determined by E_b^{Cl} alone. The low-resistance electrical continuity between the limiting membranes displaces ψ_a from E_a^K and ψ_b from E_b^{Cl}. At the apical membrane, this establishes a driving force $(E_a^K + \psi_a)$ for K secretion and, at the basolateral membrane, a driving force $-(E_b^{Cl} + \psi_b)$ for Cl absorption.

Estimation of the Membrane Conductances

It is useful to compare the calculated values of G_a and G_b with the conductances required for K and Cl diffusion across the apical and basolateral membranes. At the apical membrane, the net driving force for K exit from cell to mucosal solution $(E_a^K + \psi_a)$ is $\sim 11 \pm 1$ mV, while the rate of K diffusion is 2–3 μeq/cm^2·h (10). This requires a G_a^K of 5–7 mS/cm^2, which is in agreement with the value of G_a (5.2 $\pm$ 1.2 mS/cm^2) derived from our analysis (Table II).

At the basolateral membrane, the net driving force for Cl exit $-(E_b^{Cl} + \psi_b)$ averaged 25 $\pm$ 2 mV, while the rate of conductive Cl exit across this barrier was 3–4 μeq/cm^2·h (6, 9, 10). This would require a G_b^{Cl} of ~ 3 mS/cm^2, which is higher than the calculated G_b (1.5 $\pm$ 0.4 mS/cm^2) by a factor of 2. This conclusion also applies to the data of Table II alone since these tissues were representative of previous studies. Thus, the calculated G_b is insufficient to account for the rate of diffusional Cl exit suggested from the results of prior flux studies (Fig. 10). This estimate of G_b can be expected to err on the low side of the required value because of distributed resistance of the paracellular pathway,[4] which tends to underestimate both f_a^R and G_c (as determined from the effect of a transepithelial K gradient on ψ_t). Thus, it is difficult to assign explicit values to the partitioning of net Cl exit between conductive and nonconductive mechanisms. Our conclusions regarding the availability of K (for coupled exit) rely on assumptions about Na/K pump stoichiometry and the extent to which apical Na/K/Cl co-transport accounts for NaCl entry. The findings presented in the companion paper suggest a component of K-independent NaCl entry, but its contribution to NaCl absorption under control conditions (to which the model of Fig. 10 applies) has not been assessed.

The inadequacy of Cl conductance pathways to account entirely for net Cl movements across the basolateral membranes of absorptive epithelia has been inferred also for *Necturus* proximal tubule (15, 33) and gallbladder (28), rabbit renal thick ascending limb (14), and rabbit gallbladder (7). Evidence for the presence of such a mechanism in *Necturus* gallbladder has recently been reported by Reuss (29). Fig. 10 depicts a model in which NaCl entry is entirely K-dependent and where the observed rate of K secretion (10) leaves little K available

(from mass balance considerations) for coupled exit with Cl. Within the constraints of this model, KCl exit makes a minor contribution to Cl absorption across the basolateral membrane. However, KCl exit becomes quantitatively significant as K-independent NaCl entry increases (16) or during reduced G_a^K, as outlined below.

Distribution of Cl Exit Between Conductive and Nonconductive Mechanisms

The finding that ~50% of ψ_t remains after blockade of the apical K conductance by mucosal Ba indicates that NaCl absorption continues under these conditions, although under modified constraints. Furosemide-sensitive active K absorption is unmasked by mucosal Ba, so that Na/K/Cl co-transport continues to operate (10). As discussed earlier, the depolarization of ψ_a (and ψ_b) induced by mucosal Ba causes ψ_b to approach E_b^{Cl}, so that the driving force for diffusional Cl exit from cell to serosal solution is eliminated (Table III). Under these conditions, KCl co-transport across the basolateral membrane may play an important role in absorption of both K and Cl, since a conductance pathway for K exit is not present (Fig. 7) and the driving force for conductive Cl exit, $-(E_b^{Cl} + \psi_b)$, is near zero. A similar conclusion may apply to those tissues with spontaneously low ψ_a and ψ_b values. Their ψ_t values suggest a significant rate of NaCl absorption, although the electrical driving force for Cl diffusion across the basolateral membrane is compromised.

The finding that tissues exhibit spontaneously low ψ_a values suggests that there may be concurrent regulation of the apical and basolateral processes responsible for K exit from the cell. A decreased G_a leads to net K absorption (10) and, perhaps, a shift in the mechanism of Cl exit across the basolateral membrane from diffusion to co-transport with K. The foregoing discussion highlights an apparent relation between co-transport pathways and apical K conductance. In addition, an alteration in the cellular conductance properties accompanies inhibition of NaCl absorption (16). The ionic basis of these effects is one subject of the companion paper.

REFERENCES

1. Armstrong, C. M., R. P. Swenson, and S. R. Taylor. 1982. Block of squid axon potassium channels by internally and externally applied barium ions. *J. Gen. Physiol.* 80:663–682.
2. Boulpaep, E., and H. Sackin. 1980. Electrical analysis of intraepithelial barriers. *In* Current Topics in Membranes and Transport. F. Bronner and A. Kleinzeller, editors. Academic Press, Inc., New York. 13:169–197.
3. Burg, M. 1982. Thick ascending limb of Henle's loop. *Kidney Int.* 22:454–464.
4. Cremaschi, D., and G. Meyer. 1982. Amiloride-sensitive sodium channels in rabbit and guinea-pig gallbladder. *J. Physiol. (Lond.).* 326:21–34.

5. Curtis, R. L., J. S. Trier, R. A. Frizzell, N. M. Linden, and J. L. Madara. 1984. Flounder intestinal absorptive cells have abundant gap junctions and may be coupled. *Am. J. Physiol.* 246(Cell Physiol. 15):C77–C83.

6. Duffey, M. E., S. M. Thompson, R. A. Frizzell, and S. G. Schultz. 1979. Intracellular chloride activities and active chloride absorption in the intestinal epithelium of the winter flounder. *J. Membr. Biol.* 50:331–341.

7. Duffey, M. E., K. Turnheim, R. A. Frizzell, and S. G. Schultz. 1978. Intracellular chloride activities in rabbit gallbladder: direct evidence for the role of the sodium-gradient in energizing "uphill" chloride transport. *J. Membr. Biol.* 42:229–239.

8. Eaton, D. C., and M. S. Brodwick. 1980. Effects of barium on the potassium conductance of squid axon. *J. Gen. Physiol.* 75:727–750.

9. Field, M., K. J. Karnaky, P. L. Smith, J. E. Bolton, and W. B. Kinter. 1978. Ion transport across the isolated intestinal mucosa of the winter flounder, *Pseudopleuronectes americanus*. I. Functional and structural properties of cellular and paracellular pathways for Na and Cl. *J. Membr. Biol.* 41:265–293.

10. Frizzell, R. A., D. R. Halm, M. W. Musch, C. P. Stewart, and M. Field. 1984. Potassium transport by flounder intestinal mucosa. *Am. J. Physiol.* 246(Renal Fluid Electrolyte Physiol. 15):F946–F951.

11. Frizzell, R. A., P. L. Smith, and M. Field. 1981. Sodium chloride absorption by flounder intestine: a model for the renal thick ascending limb. *In* Membrane Biophysics: Structure and Function in Epithelia. M. Dinno and A. Callahan, editors. Alan R. Liss, New York. 67–81.

12. Gogelein, H., and W. Van Driessche. 1981. Noise analysis of the potassium current through the apical membrane of *Necturus* gallbladder. *J. Membr. Biol.* 60:187–198.

13. Greger, R., and E. Schlatter. 1983. Properties of the lumen membrane of the cortical thick ascending limb of Henle's loop of rabbit kidney. *Pflügers Arch. Eur. J. Physiol.* 396:315–324.

14. Greger, R., and E. Schlatter. 1983. Properties of the basolateral membrane of the cortical thick ascending limb of Henle's loop of rabbit kidney: a model for secondary active chloride transport. *Pflügers Arch. Eur. J. Physiol.* 396:325–374.

15. Guggino, W. B., E. L. Boulpaep, and G. Giebisch. 1982. Electrical properties of chloride transport across the *Necturus* proximal tubule. *J. Membr. Biol.* 65:185–196.

16. Halm, D. R., E. J. Krasny, Jr., and R. A. Frizzell. 1985. Electrophysiology of flounder intestinal mucosa. II. Relation of the electrical potential profile to coupled NaCl absorption. *J. Gen. Physiol.* 85:865–883.

17. Hebert, S. C., and T. E. Andreoli. 1984. Control of NaCl transport in the thick ascending limb. *Am. J. Physiol.* 246(Renal Fluid Electrolyte Physiol. 15):F745–F756.

18. Helman, S. I., and K. W. Beyenbach. 1978. Electrophysiological study of the apical barrier of the intestinal epithelium of winter flounder (*Pseudopleuronectes americanus*). *Bull. Mt. Desert Isl. Biol. Lab.* 18:51–54.

19. Koeppen, B. M., B. A. Biagi, and G. H. Giebisch. 1983. Intracellular microelectrode characterization of the rabbit cortical collecting duct. *Am. J. Physiol.* 244(Renal Fluid Electrolyte Physiol. 13):F35–F47.

20. Krasny, E. J., Jr., and R. A. Frizzell. 1984. Intestinal ion transport in marine teleosts. *In* Chloride Transport Coupling in Biological Membranes and Epithelia. G. A. Gerencer, editor. Elsevier/North Holland, New York. 205–220.

21. Krasny, E. J., Jr., J. Madara, D. R. DiBona, and R. A. Frizzell. 1983. Cyclic-AMP regulates tight junction permselectivity in flounder intestine. *Fed. Proc.* 42:1100. (Abstr.)

22. Lewis, S. A., D. C. Eaton, and J. M. Diamond. 1976. The mechanism of sodium transport by rabbit urinary bladder. *J. Membr. Biol.* 28:41–70.

23. Macknight, A. D. C., D. R. DiBona, and A. Leaf. 1980. Sodium transport across toad urinary bladder: a model "tight" epithelium. *Physiol. Rev.* 60:615–715.

24. Musch, M. W., S. A. Orellana, L. S. Kimberg, M. Field, D. R. Halm, E. J. Krasny, Jr., and R. A. Frizzell. 1982. Na:K:Cl cotransport in the intestine of a marine teleost. *Nature (Lond.).* 300:351–353.

25. Musch, M. W., M. C. Rao, M. Field, D. R. Halm, and R. A. Frizzell. 1983. Potassium influx across flounder intestinal brush border: sodium and chloride dependence and effect of ouabain. *Fed. Proc.* 42:988. (Abstr.)

26. Nagel, W. 1979. Inhibition of potassium conductance by barium in frog skin epithelium. *Biochim. Biophys. Acta.* 552:346–357.

27. Oberleithner, H., G. Giebisch, F. Lang, and W. Wang. 1982. Cellular mechanism of the furosemide-sensitive transport system in the kidney. *Klin. Wochenschr.* 60:1173–1179.

28. Reuss, L. 1979. Electrical properties of the cellular transepithelial pathway in *Necturus* gallbladder. III. Ionic permeability of the basolateral cell membrane. *J. Membr. Biol.* 47:239–259.

29. Reuss, L. 1983. Basolateral K:Cl co-transport in a Na:Cl-absorbing epithelium. *Nature (Lond.).* 305:723–726.

30. Reuss, L., L. Y. Cheung, and J. P. Grady. 1981. Mechanisms of cation permeation across apical cell membrane of *Necturus* gallbladder: effects of luminal pH and divalent cations on potassium and sodium permeability. *J. Membr. Biol.* 59:211–224.

31. Reuss, L., and A. L. Finn. 1975. Electrical properties of the cellular transepithelial pathway in *Necturus* gallbladder. I. Current analysis and steady-state effects of mucosal solution ionic substitutions. *J. Membr. Biol.* 25:115–139.

32. Schultz, S. G. 1979. Principles of electrophysiology and their application to epithelial tissues. *In* MTP International Review of Science: Gastrointestinal Physiology. E. D. Jacobson and L. L. Shanbour, editors. University Park Press, Baltimore, MD. 4:69–104.

33. Shindo, T., and K. Spring. 1981. Chloride movement across the basolateral membrane of proximal tubule cells. *J. Membr. Biol.* 58:35–42.

34. Smith, P. L., M. J. Welsh, C. P. Stewart, R. A. Frizzell, S. A. Orellana, and M. Field. 1980. Chloride absorption by the intestine of the winter flounder *Pseudopleuronectes americanus*: mechanism of inhibition by reduced pH. *Bull. Mt. Desert Isl. Biol. Lab.* 20:96–101.

35. Stewart, C. P., P. L. Smith, M. J. Welsh, R. A. Frizzell, M. Musch, and M. Field. 1980. Potassium transport by the intestine of the winter flounder, *Pseudopleuronectes americanus*: evidence for KCl co-transport. *Bull. Mt. Desert Isl. Biol. Lab.* 20:92–96.

36. Suzuki, K., G. Kottra, L. Kampmann, and E. Fromter. 1982. Square wave pulse analysis of cellular and paracellular conductance pathways in *Necturus* gallbladder epithelium. *Pflügers Arch. Eur. J. Physiol.* 394:302–312.